

On the Utility of Koopman Operator Theory in Learning Dexterous Manipulation Skills

Yunhai Han*, Mandy Xie*, Ye Zhao*, and Harish Ravichandar*

*Institute for Robotics and Intelligent Machines

Georgia Institute of Technology, Atlanta, Georgia 30332-0250

Email: {yhan389, manxie, yezhao, harish.ravichandar}@gatech.edu

Abstract—Recent advances in learning-based approaches have led to impressive dexterous manipulation capabilities. Yet, we haven’t witnessed widespread adoption of these capabilities beyond the laboratory. This is likely due to practical limitations, such as significant computational burden, inscrutable policy architectures, sensitivity to parameter initializations, and the considerable technical expertise required for implementation. In this work, we investigate the utility of Koopman operator theory in alleviating these limitations. Koopman operators are simple yet powerful control-theoretic structures that help represent complex nonlinear dynamics as *linear* systems in higher-dimensional spaces. Motivated by the fact that complex nonlinear dynamics underlie dexterous manipulation, we develop an imitation learning framework that leverages Koopman operators to simultaneously learn the desired behavior of both robot and object states. We demonstrate that a Koopman operator-based framework is surprisingly effective for dexterous manipulation and offers a number of unique benefits. First, the learning process is *analytical*, eliminating the sensitivity to parameter initializations and painstaking hyperparameter optimization. Second, the learned reference dynamics can be combined with a *task-agnostic* tracking controller such that task changes and variations can be handled with ease. Third, a Koopman operator-based approach can perform comparably to state-of-the-art imitation learning algorithms in terms of task success rate and imitation error, while being *an order of magnitude* more computationally efficient. In addition, we discuss a number of avenues for future research made available by this work.

I. INTRODUCTION

Autonomous dexterous manipulation is a necessary skill for robots operating in a physical world built by and for humans. However, achieving reliable and generalizable dexterous manipulation skills has been a long-standing challenge [1] due to numerous factors, such as complex nonlinear dynamics, high-dimensional action spaces, and difficulties in designing bespoke controllers that do not generalize to task variations.

Over the past decade, learning-based solutions are beginning to emerge as a promising solution that can address the challenges in acquiring dexterous manipulation skills. Indeed, these methods have been shown to be capable of impressive feats, such as solving Rubik’s cubes [2], manipulation baoding balls [3], and retrieving tool trays [4].

However, existing learning approaches suffer from practical limitations that hinder their widespread adoption. First, implementing existing algorithms requires significant technical expertise and modern machine learning infrastructure. Second, training policies consume significant computational resources.

Third, existing approaches demand painstaking effort in tuning hyperparameters to achieve acceptable performance. Fourth, performance tends to be highly sensitive to parameter initialization. See Section II for a detailed discussion of related work.

In this work, we investigate the utility of Koopman operator theory in alleviating the limitations of existing learning-based approaches as identified above. The Koopman operator theory helps represent arbitrary nonlinear dynamics in finite dimensional spaces as linear dynamics in an infinite-dimensional Hilbert space [5]. Indeed, while this equivalence is exact and fascinating from a theoretical standpoint, it is not directly applicable in practice. However, recent advances have resulted in Koopman operator-based approaches that approximate this equivalence in high, but finite, dimensional spaces by learning the operator directly from data.

We develop a novel imitation learning algorithm, dubbed as *Koopman Operator-based Dexterous Manipulation (KODex)*, to evaluate the effectiveness and benefits of using Koopman operator theory for dexterous manipulation (see Fig. 1 for a block diagram). Specifically, we model desired behaviors as solutions to *nonlinear* dynamical systems and learn Koopman operators that define approximately-equivalent *linear* dynamics in higher-dimensional spaces. While we use polynomial functions to lift the state space in this work, KODex is agnostic to the specific lifting function. A unique aspect of dexterous manipulation is that it is object-centered [1], and the desired motion of the robot has to depend on the object state. As such, KODex *simultaneously* learns the desired motions of both the robot and the object from demonstrations. KODex then relies on a learned inverse dynamics tracking controller to generate actions that can track the reference trajectory generated by the learned reference dynamics. Note that the tracking controller is *task-agnostic*, and as such, can be preserved even if we wish to learn an entirely new task on the same robot platform.

A number of reasons motivate our exploration of Koopman operator theory within the context of dexterous manipulation. A significant benefit of learning Koopman operators from data is that it lends itself to an *analytical* solution. As such, KODex is simple to implement and does not require expertise and familiarity with state-of-the-art (SOTA) machine learning infrastructure. More importantly, KODex incurs significantly lower computational costs compared to existing approaches, and does not rely on hyperparameters that have to be painstakingly tuned by an expert. Further, KODex offers consistent

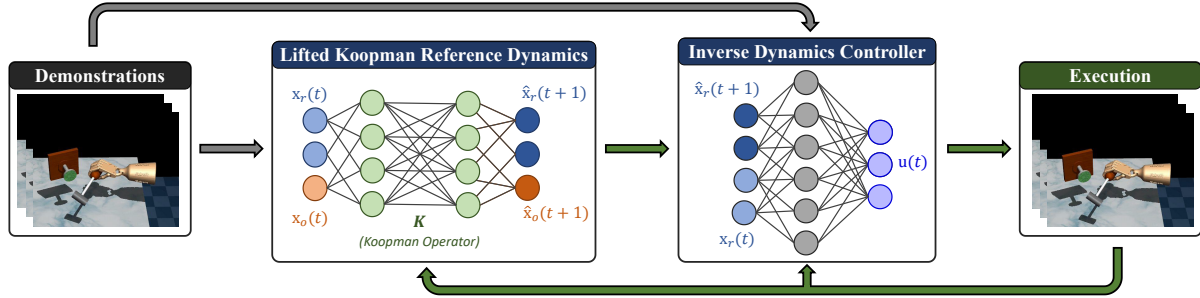


Fig. 1: KODex simultaneously encodes complex nonlinear dynamics of the desired motion of both the robot state (x_r) and the object state (x_o) as a *linear* dynamical system in a higher-dimensional space by learning a Koopman operator K directly from demonstrations. Further, KODex learns an inverse dynamics controller to track the robot reference trajectory ($\{\hat{x}_r(t)\}_{t=1}^T$) generated by the lifted linear system.

and predictable performance since the learning process is analytical and thus not sensitive to parameter initializations. Finally, given that KODex learns a *linear* dynamical system, it enables an easy inspection of the learned dynamics via a wide array of control theoretic tools.

We carry out extensive evaluations of KODex within the context of four dexterous manipulation skills on the simulated Adroit hand, an established experimental platform for dexterous manipulation [6]. Further, we compare KODex against SOTA imitation learning approaches in terms of general efficacy, training efficiency, sample efficiency, and robustness to changes to physical properties that could result from sim-to-real gap or task variations. Our results demonstrate that KODex is more computationally efficient than SOTA approaches by *an order of magnitude* or more, while achieving comparable sample efficiency and task success rate. These results suggest that Koopman operator theory has the potential to be an effective, computationally-efficient, and reliable tool to learn dexterous manipulation skills, and to reduce the barriers to adoption.

II. RELATED WORK

In this section, we discuss related work from different subfields of robotics and their connection to our work.

A. Learning Manipulation Skills as Dynamical Systems

Our work falls into the category of dynamical-system-based imitation learning methods for manipulation (see Ravichandar et al. [7] for a detailed discussion). Made popular by the seminal Dynamics Movement Primitives (DMPs) [8], these methods model robot motions as solutions to an underlying dynamical system which can be learned from demonstrations. The past decade saw a plethora of approaches that have built upon the same principle (e.g., [9–14]), creating increasingly capable LfD tools for manipulation. Robustness to perturbations, high sample efficiency, and provable convergence are all but a few examples of the many advantages of dynamical-system-based approaches. These approaches are highly structured and leverage control-theoretic and topological tools to learn complex desired motions from demonstrations in a highly sample efficient manner. In fact, most of these approaches have

demonstrated that goal-directed motions can be learned from as few as six demonstrations. More recently, Bahl et al. [15] developed Neural Dynamic Policy (NDP) which embeds the dynamical systems structure into deep neural network-based policies to enable end-to-end learning. However, a common limitation of these approaches is that they were designed to capture end-effector skills for serial-link manipulators. As such, they deal with low-dimensional systems with limited degrees-of-freedom (DOFs). We discuss a few recent exceptions to this limitation in Section II-B. In contrast, our work investigates the utility of Koopman operators in learning dexterous manipulation skills on high-DOF platforms. Further, existing dynamical-system approaches rely on expertly-designed hyperparameters and their efficacy is sensitive to parameter initializations. On the contrary, Koopman operators can be learned *analytically* from demonstrations, alleviating the dependence on painstaking hyperparameter tuning and unreliable numerical optimization.

B. Learning Dexterous Manipulation Skills

Deep Reinforcement Learning (RL) has been dominating the field of dexterous manipulation recently, enabling a variety of impressive autonomous dexterous manipulation skills. One of the most popular approaches, developed by OpenAI et al. [2], demonstrated that a high-DOF multi-finger hand can learn to solve the Rubik’s cube. More recently, Chen et al. [16] developed a model-free RL framework that was capable of reorienting over 2000 geometrically different objects and showed strong zero-shot transfer to new objects. Along similar lines, several recent approaches have demonstrated the effectiveness of RL for dexterous manipulation [3, 17, 18]. Despite their impressive successes, RL-based algorithms suffer from poor sample efficiency and their policies are notoriously difficult to train. In contrast, Imitation learning (IL) aims to improve sample efficiency by leveraging expert demonstrations [19, 7]. However, most existing IL-based methods (including those discussed in Sec. II-B) focus on lower-DOF manipulators and do not scale well to high-dimensional systems. Indeed, there are at least two recent notable exceptions to this limitation. Xie et al. [4] developed a highly structured IL method to learn dexterous manipulation skills from demonstrations in

the form of a dynamical system. Arunachalam et al. [20] introduced a mixed-reality framework that can collect high-quality demonstrations and learn dexterous manipulation skills by leveraging visual representations and motion retargeting. Recent work has also attempted to combine IL with RL in efforts to get the best of both approaches and has been able to achieve impressive performance (e.g., [21, 6]). A common attribute of existing learning methods to dexterous manipulation, irrespective of whether they leverage RL, IL, or both, is that they rely on large neural networks that have to be trained via numerical optimization. As a result, training typically requires considerable computational resources and relies on significant user expertise for implementation, and hyperparameter tuning. Furthermore, the effectiveness of their approaches is highly sensitive to parameter initialization [22]. In stark contrast, KODex encodes complex skills as linear dynamical systems that can be learned analytically from demonstrations. As such, KODex demands significantly fewer computational resources and is not sensitive to parameter initialization. Further, unlike opaque deep neural networks, KODex learns a linear dynamical system that can be inspected via a wide array of control-theoretic tools.

C. Koopman Operator for Robotics

Recently, Koopman operator theory has been applied to various robotic systems. It has been shown that learning Koopman operators can enable model-based control of differential drive mobile robots [23], and data-driven control of spherical and serial-link manipulator robots [24]. Recent approaches have also shown that it is possible to model and control a soft robot manipulator using Koopman operator [25, 26]. However, the robotic systems investigated in these works are low-dimensional and have limited DOFs. In contrast, our work is focused on evaluating the effectiveness of Koopman operators in learning skills for a high-dimensional robotic system with more complex dynamics (e.g. a multi-finger dexterous hand). Further, prior works have not presented rigorous comparisons of their Koopman-based methods against SOTA learning methods built upon neural network architectures. As such, we do not yet fully understand the benefits of leveraging Koopman operator when comparing to SOTA learning approaches, and the circumstances under which these benefits hold. In our work, we thoroughly evaluate KODex against SOTA imitation learning methods within the context of four dexterous manipulation tasks in terms of various performance metrics.

III. PRELIMINARY: KOOPMAN OPERATOR THEORY

We begin by providing a brief introduction to Koopman operator theory – a control-theoretic approach used to represent nonlinear dynamical systems as a linear system of equations [5].

A. Koopman Operator Representation

Consider a discrete-time autonomous nonlinear dynamical system whose state evolution is defined by

$$\mathbf{x}(t+1) = F(\mathbf{x}(t)), \quad (1)$$

where $\mathbf{x}(t) \in \mathcal{X} \subset \mathbb{R}^n$ represents the system state at time t , and $F(\cdot)$ is an arbitrary nonlinear mapping: $\mathbb{R}^n \rightarrow \mathbb{R}^n$.

To represent the the nonlinear dynamical system in (1) as a linear system, we can begin by introducing a set of *observables* using the so-called *lifting function* $g : \mathcal{X} \rightarrow \mathcal{O}$, where \mathcal{O} is the space of observables. We can now define the *Koopman Operator* \mathcal{K} , an infinite-dimensional operator on the lifting function $g(\cdot)$ as follows

$$[\mathcal{K}g] = g \circ F(\mathbf{x}(t)) \quad (2)$$

where \circ is the compositional operator. For the discrete time system defined in (1), the above equation can be rewritten as

$$[\mathcal{K}g] = g(F(\mathbf{x}(t))) = g(\mathbf{x}(t+1)) \quad (3)$$

If the observables belong to a vector space, the Operator \mathcal{K} can be seen as an infinite-dimensional linear map that describes the evolution of the observables as follows

$$g(\mathbf{x}(t+1)) = \mathcal{K}g(\mathbf{x}(t)) \quad (4)$$

Therefore, the Koopman operator \mathcal{K} linearly propagates forward the infinite-dimensional lifted states (i.e., observables).

In practice, we do not benefit from this representation since it is infinite-dimensional. However, we can approximate \mathcal{K} using a matrix $\mathbf{K} \in \mathbb{R}^{p \times p}$ and define a finite set of observables $\phi_t = g(\mathbf{x}(t)) \in \mathbb{R}^p$. Thus, we can rewrite the relationship in (4) as

$$g(\mathbf{x}(t+1)) = \mathbf{K}g(\mathbf{x}(t)) + r(\mathbf{x}(t)), \quad (5)$$

where $r(\mathbf{x}(t)) \in \mathbb{R}^p$ is the residual error caused by the finite dimensional approximation, which can be arbitrarily reduced based on the choice of p .

B. Learning Koopman Operator from Data

Given a choice of observables, it is possible to learn the matrix operator \mathbf{K} directly from a dataset $D = [\mathbf{x}(1), \mathbf{x}(2), \dots, \mathbf{x}(T)]$, which contains the solution to the system in (1) for T time steps.

Given the choice of $g(\cdot)$, the finite dimensional Koopman matrix \mathbf{K} can now be determined by minimizing the approximation error defined in (5). Specifically, we can obtain \mathbf{K} from D by minimizing the cost function $\mathbf{J}(\mathbf{K})$ given below

$$\begin{aligned} \mathbf{J}(\mathbf{K}) &= \frac{1}{2} \sum_{t=1}^{t=T-1} \|r(\mathbf{x}(t))\|^2 \\ &= \frac{1}{2} \sum_{t=1}^{t=T-1} \|g(\mathbf{x}(t+1)) - \mathbf{K}g(\mathbf{x}(t))\|^2 \end{aligned} \quad (6)$$

Note minimizing $\mathbf{J}(\mathbf{K})$ amounts to solving a least-square problem, whose solution is given by [27]

$$\mathbf{K} = \mathbf{A}\mathbf{G}^\dagger \quad (7)$$

where \mathbf{G}^\dagger denotes the Moore–Penrose inverse of \mathbf{G} , and

$$\begin{aligned} \mathbf{A} &= \frac{1}{T-1} \sum_{t=1}^{t=T-1} g(\mathbf{x}(t+1)) \otimes g(\mathbf{x}(t)) \\ \mathbf{G} &= \frac{1}{T-1} \sum_{t=1}^{t=T-1} g(\mathbf{x}(t)) \otimes g(\mathbf{x}(t)) \end{aligned} \quad (8)$$

where \otimes denotes the outer product between two vectors.

IV. LEARNING KOOPMAN OPERATORS FOR DEXTEROUS MANIPULATION

In this section, we introduce our learning framework KODex. We begin by introducing our framework to model dexterous manipulation skills as nonlinear dynamics and discuss the importance of incorporating object states into the system (Section IV-A). Next, we describe how KODex learns the reference dynamics for a given skill from demonstrations (Section IV-B). Finally, we discuss how to learn a low-level controller, also from demonstrations, in order to faithfully track the reference trajectories generated by KODex (Section IV-C). Further, an overall pseudo-code for KODex can be found in Algorithm 1.

A. Modeling Dexterous Manipulation Skills

A central principle behind KODex is that the desired behavior of a robot can be represented using a dynamical system. Note that, unlike other kinds of manipulation skills (e.g., end-effector skills of multi-link manipulators), dexterous manipulation is explicitly concerned with how an object moves as a result of the robot's motion [1]. As such, KODex captures the desired motion of the robot along with that of the object. To this end, we define the state at time t as $\mathbf{x}(t) = [\mathbf{x}_r(t)^\top, \mathbf{x}_o(t)^\top]^\top$, where $\mathbf{x}_r(t) \in \mathcal{X}_r \subset \mathbb{R}^n$ and $\mathbf{x}_o(t) \in \mathcal{X}_o \subset \mathbb{R}^m$ represent the state of the robot and the object, respectively, at time t . As such, the dynamical system we wish to capture is

$$\mathbf{x}(t+1) = F^*(\mathbf{x}(t)) \quad (9)$$

where $F^*(\cdot) : \mathcal{X}_r \times \mathcal{X}_o \rightarrow \mathcal{X}_r \times \mathcal{X}_o$ denotes the true dynamics that govern the *interdependent* motions of the robot and the object. Note that the dynamical system above is time-invariant. Indeed, it has been demonstrated that time-invariant dynamical systems provide a natural way to capture manipulation skills that is more robust to intermittent perturbations than those that explicitly depend on time [7].

A key challenge in learning the dynamical system in (9) is that it can be arbitrarily complex and highly nonlinear, depending on the particular skill of interest. KODex leverages Koopman operator theory to learn a *linear* dynamical system that can effectively approximate such complex dynamics. To this end, we first define a set of observables through the lifting function $g(\mathbf{x})$ as follows

$$g(\mathbf{x}(t)) = [\mathbf{x}_r(t)^\top, \psi_r(\mathbf{x}_r(t)), \mathbf{x}_o(t)^\top, \psi_o(\mathbf{x}_o(t))]^\top, \forall t \quad (10)$$

where $\psi_r : \mathbb{R}^n \rightarrow \mathbb{R}^{n'}$ and $\psi_o : \mathbb{R}^m \rightarrow \mathbb{R}^{m'}$ are vector-valued lifting functions that transform the robot and object state respectively. Now, the linear dynamical system in the space of observables will take the same form as in (5).

In our implementation, we use polynomial functions up to a finite degree in our lifting function since polynomial functions allow for flexible definition of complex functions. However, it is important to note that KODex is agnostic to the specific choice of observables. Further, we do not assume that we know

the ideal set of observables for any given skill. Instead, as we demonstrate in Section VI, KODex can learn different skills on the same space of observables.

B. Learning Reference Dynamics

We now turn to the challenge of learning the Koopman operator \mathbf{K} from demonstrations. Let $D = [\{\mathbf{x}^{(1)}(t), \tau^{(1)}(t)\}_{t=1}^{T^{(1)}}, \dots, \{\mathbf{x}^{(N)}(t), \tau^{(N)}(t)\}_{t=1}^{T^{(N)}}]$ denote a set of N demonstrations containing trajectories of state-torque pairs. Now, we can compute the Koopman matrix as $\mathbf{K} = \mathbf{A}\mathbf{G}^\dagger$, where \mathbf{A} and \mathbf{G} can be computed by modifying (8) as follows

$$\begin{aligned} \mathbf{A} &= \sum_{n=1}^{n=N} \sum_{t=1}^{t=T^{(n)}-1} \frac{g(\mathbf{x}^n(t+1)) \otimes g(\mathbf{x}^n(t))}{N(T^{(n)}-1)} \\ \mathbf{G} &= \sum_{n=1}^{n=N} \sum_{t=1}^{t=T^{(n)}-1} \frac{g(\mathbf{x}^n(t)) \otimes g(\mathbf{x}^n(t))}{N(T^{(n)}-1)} \end{aligned} \quad (11)$$

It is worth noting that KODex can also leverage partial trajectories that do not complete the task, as long as all the state pairs $(\mathbf{x}^n(t), \mathbf{x}^n(t+1))$ are temporally consecutive. Additionally, we also record the actuated torque $\tau(t)$ at each time step for the controller design discussed in Section IV-C.

Once the reference dynamics are learned, we will be able to integrate it to generate a rollout in the observables space. However, in order to command the robot, we need to obtain the rollouts in the original robot states. Recall from Eq. (10) that we designed $g(\mathbf{x}(t))$ such that both robot state $\mathbf{x}_r(t)$ and object state $\mathbf{x}_o(t)$ are part of the observables. As such, we can retrieve the desired robot state trajectory $\{\hat{\mathbf{x}}_r(t)\}$ by selecting the corresponding elements in $g(\mathbf{x}(t))$.

Indeed, the data distribution in D has a considerable effect on the generalizability of the computed Koopman matrix \mathbf{K} . Therefore, there is an inevitable trade-off between the number of demonstrations and the cost of data collection - a challenge shared by most imitation learning algorithms.

C. Learning the Controller

To track the desired trajectories generated from the learned reference dynamics, we design an inverse dynamics controller C [28] [15], which takes as input the current robot state $\mathbf{x}_r(t)$ and the desired next state from the reference trajectory $\hat{\mathbf{x}}_r(t+1)$, and generates the torque $\tau(t)$ required for actuation. The robot state can be read from simulators or robot sensors.

We use a multi-layer perception (MLP) to parameterize the tracking controller and train it with supervision using the recorded state-torque pairs $(\mathbf{x}_r^n(t), \mathbf{x}_r^n(t+1), \tau^n(t))$ from the demonstrations. In other words, we minimize:

$$\mathcal{L}_{\text{control}} = \sum_{n=1}^{n=N} \sum_{t=1}^{t=T^{(n)}-1} \frac{|C(\mathbf{x}_r^n(t), \mathbf{x}_r^n(t+1)) - \tau^n(t)|^2}{N(T^{(n)}-1)} \quad (12)$$

Note that the controller can also be trained without the demonstrations by collecting self-play data. Indeed, it has been shown that it is possible to separately train a controller via

Algorithm 1: KODex**Demonstration Data Collection**

```
Initialize  $D = \emptyset$ ;  
for  $n \in \{1, \dots, N\}$  do  
    Generate a  $T^{(n)}$ -horizon trajectory of states and  
    torques  $\{[x^n(t), \tau^n(t)]\}_{t=1}^{T^{(n)}}$ ;  
    Add  $\{[x^n(t), \tau^n(t)]\}_{t=1}^{T^{(n)}}$  to  $D$ ;  
end
```

Koopman Operator Approximation

```
Determine lifting function  $g(x(t))$ ;  
Compute  $\mathbf{K}$  on  $D$  (7, 11);
```

Controller Design

```
Build a controller  $C$  as a neural network with inputs  
as  $(x_r(t), x_r(t+1))$  and output as  $\tau(t)$ ;
```

```
Train  $C$  using state-torque pairs  
 $(x_r^n(t), x_r^n(t+1), \tau^n(t))$  in  $D$  (12);
```

Implementation

```
Specify the initial states  $x(1)$ ;
```

```
for  $t \in \{1, \dots, T-1\}$  do  
    Predict the next robot states  $\hat{x}_r(t+1)$  using  $\mathbf{K}$  (4  
    10);  
    Read the current robot states  $x_r(t)$ ;  
    Generate the torque  $\tau(t)$  using  $C$  on  
     $(x_r(t), \hat{x}_r(t+1))$  and execute it;  
end
```

reinforcement learning to track the reference trajectories [29]. Note that KODex does not require torque information to learn the reference dynamics. As such, if the controller is training from self-play data, KODex can learn skills from state-only observations [30].

D. Execution

With the reference dynamics and the tracking control learned, we detail how we execute the policy in this section. Now, suppose $x(1) = (x_r(1), x_o(1))$ is the given initial state, we can then generate the reference trajectory $(\{\hat{x}_r(t)\}_{t=1}^T)$ by integrating the learned reference dynamics. Further, at time step t , we pass the current robot state $x_r(t)$ and the desired next robot state $\hat{x}_r(t+1)$ to the controller C to compute the required torque $\tau(t)$.

V. EXPERIMENTAL DESIGN

To evaluate KODex and compare it to existing approaches, we designed and carried out a series of experiments. We designed our experiments on KODex in terms of its i) general efficacy (Sec. VI-A), ii) sample efficiency (Sec. VI-B), iii) Out-of-distribution generalization (Sec. VI-C), and iv) robustness to changes in physical properties (Sec. VI-D).

A. Evaluation Platform

We conducted all our experiments on the widely-used ADROIT Hand [6] – a 30-DoF simulated system (24-DoF hand + 6-DoF floating wrist base) built with MuJoCo [31].

B. Baselines

We compared KODex against the following baselines:

- *NN*: A fully-connected Neural Network policy
- *LSTM*: A recurrent neural network policy with Long Short-Term Memory units
- *NDP*: An Neural Dynamic policy [15]
- *NGF*: An Neural Geometric Fabrics policy [4]

Note that the NN and LSTM represent unstructured baselines that serve to investigate the need for structured policies. NDP and NGF are highly structured policies that serve as SOTA imitation learning baselines for manipulation.

We undertook several precautions to ensure a fair comparison. First, we designed the robot and object state space for all baselines and KODex to be identical. Second, we carefully designed the baselines policies and tuned their hyper-parameters for each baseline method as details in Appendices VII-D and VII-E. Third, we trained each baseline method over five random seeds for each task to control for initialization effects. For all tasks, we saved the baseline policies that performed the best on a validation set of 50 held-out demonstrations. Note that KODex utilizes an analytical solution and thus does not require parameter initialization or hyper parameter optimization.

C. Tasks

We evaluated KODex and the baselines on the same set of four tasks originally proposed in [6] (see Fig. 2).

- *Tool use*: Pick up the hammer to drive the nail into the board placed at a randomized height.
- *Door opening*: Given a randomized door position, undo the latch and drag the door open.
- *Object relocation*: Move the blue ball to a randomized target location indicated by the green sphere.
- *In-hand reorientation*: Given a randomized goal orientation represented by the green pen, reorient the blue pen to the goal orientation.

See Appendix VII-A for the state space design of all tasks.

D. Metrics

We use the following metrics to quantify the performance of KODex and that of the baseline methods:

- *Training time*: The number of seconds taken by each method to train a policy.
- *Imitation error*: The difference (L1-norm) between robot joint trajectories generated by the learned policy and the demonstrations when initialized at the same configuration.
- *Task success rate*: The percentage of trials in which the task was successfully performed by the learned policy (see Appendix VII-B for the specific success criteria).

Further, we investigate each method’s *sample efficiency* by reporting how the above metrics vary as a function of the number of demonstrations.

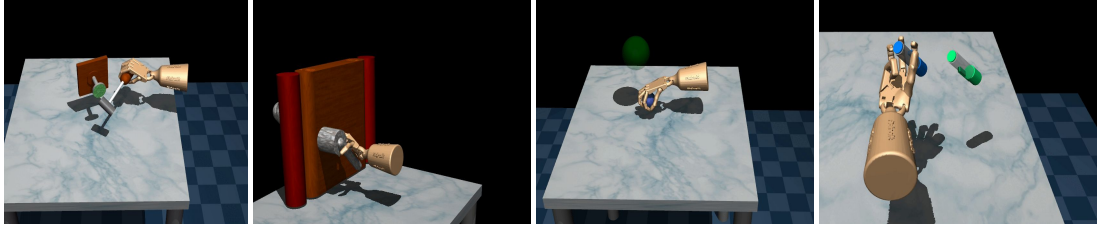


Fig. 2: We evaluate KODex on four tasks from [6]. *Left to right*: Tool Use, Door Opening, Object Relocation, and In-hand Reorientation.

E. Expert Policy

For each task, we trained an expert RL agent using DAPG as described in [6] and collected 250 successful rollouts as expert demonstrations (200 for training and 50 for validation). See Appendix. VII-C for a more detailed description of the sampling procedure.

F. Inverse Dynamics Controller

To standardize controller performance across methods, we first trained a common inverse dynamics controller for each task using the 250 demonstrations (see Appendix. VII-F).

VI. RESULTS AND DISCUSSION

In this section, we report the results from the experiments that were setup as discussed in the previous section. We evaluate KODex on its i) general efficacy, ii) sample efficiency, iii) out-of-distribution generalization, and iv) robustness to changes in physical properties of the robot and the object.

A. General Efficacy

We generated 200 new rollouts with the expert RL policy (within the same distribution as the demonstrations) as the test set. In Fig. 3, we report the training time, imitation error, and task success rate for each method on each task, when trained on 200 demonstrations and tested on the new 200 testing instances.

Training time: As can be seen, KODex takes a significantly (by an order of magnitude) shorter time to train a policy compared to both unstructured baselines (NN, LSTM) and SOTA IL methods (NDP, NGF). Further, this trend holds across all the tasks. This is to be expected since KODex analytically computes the Koopman operator unlike all the baselines, which rely on gradient descent and numerical optimization.

Imitation error: We have excluded the significantly larger imitation errors generated by NN from the plot in order to preserve necessary resolution to distinguish between the performance of other methods. In general, all methods (except NN) achieve low imitation error for the Tool Use task with a minimal difference across methods. In the three remaining tasks, we see that all structured methods (NDP, NGF, KODex) considerably outperform the unstructured baseline (LSTM). These results reinforce the effectiveness of structured methods in imitating demonstrations. Importantly, these results suggest that KODex, despite its simplicity, is able to achieve imitation performance comparable to the SOTA IL methods, while remaining an order of magnitude more computationally efficient.

Task success rate: As one would expect, the naive NN policy performs significantly worse than all other methods. On the other hand, LSTM achieves impressive task success rates, even outperforming NDP in two of the four tasks. This is in stark contrast to its high imitation error. While counter-intuitive at first, this observation is not surprising given the recent finding that a low imitation error does not necessarily translate to a high task success rate [32]. We observe that KODex and NGF perform comparably, with one achieving a higher task success rate than the other in two of the four tasks. Importantly, KODex results in the most consistent and predictable performance due to its analytical nature and free of sensitivity to initialization.

B. Sample Efficiency

To investigate sample efficiency, we trained policies on a varying number of demonstrations ([10, 25, 50, 100, 150, 200]). In Fig. 4, we report the training time, imitation error, and task success rate for each method as a function of the number of demonstrations when tested on the same 200 test instances used to evaluate general efficacy.

Training time: A key observation from these plots is that, KODex’s training time increases at a significantly lower rate compared to the baselines as we increase the number of demonstrations, suggesting that KODex scales much better than the baselines.

Imitation error and Task success rate: We find that unstructured models (NN and LSTM) fail to demonstrate a consistent monotonic decrease (increase) in imitation error (task success rate) as we increase the number of demonstrations. In stark contrast, structured methods (NDP, NGF, and KODex) are able to leverage additional demonstrations to consistently drive down imitation errors and improve task success rates. KODex almost consistently achieves the lowest imitation error and highest task success rate with the fewest number of demonstrations, which is closely followed by NGF. These observations suggest that KODex tends to be more sample efficient than the baselines. This superior performance is likely due to the rich structure induced by the Koopman operator theory and the resulting effectiveness in capturing nonlinear dynamics. The only exception to this trend is observed for the Object Relocation task, in which KODex requires 150 demonstrations to perform comparably well to the other structured methods (NDP, NGF). We conjecture this is due to the fact that the hand base needs to move across a large task space for this

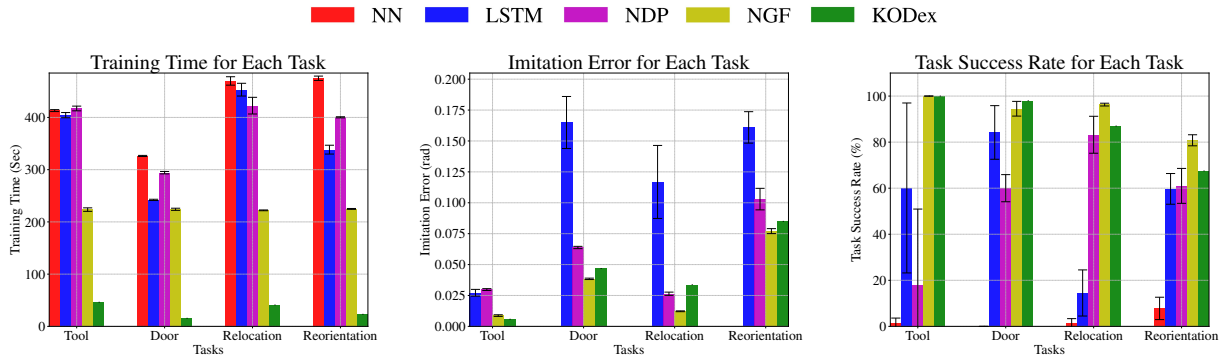


Fig. 3: Policy performances on all tasks based on three metrics: Training Time (left figure), Imitation Error (middle figure), and Task Success Rate (right figure). Each method was trained on 200 demonstrations and evaluated on the test set. For baseline methods, the error bars show the standard deviation over five random seeds. Note that we did not plot NN’s imitation errors as they were out of scale.

TABLE I: Out-of-distribution task success rates

Success Rate (%)	Task	Tool	Door	Relocation	Reorientation
Policy					
NN	0.0(±0.0)	0.0(±0.0)	0.0(±0.0)	14.2(±9.5)	
LSTM	24.6(±16.0)	20.9(±12.1)	2.6(±5.0)	48.3(±2.2)	
NDP	35.8(±4.2)	11.3(±1.7)	73.4(±14.2)	53.9(±3.3)	
NGF	42.7(±10.9)	29.8(±3.9)	97.7(±3.4)	63.6(±7.6)	
KODex	61.5	30.5	66.0	33.0	
Expert	99.0	31.5	100.0	51.5	

task and thus the trajectories exhibit high-variance in the demonstrations.

C. Out-of-Distribution Generalization

We generated a new set of 200 out-of-distribution samples to evaluate how the policies that were trained on 200 demonstrations generalize to unseen samples (see Appendix. VII-C for more details). In Table I, we report the task success rates of each method trained on 200 demonstrations and tested on 200 out-of-distribution samples. In addition, we also report the task success rate of the expert policy on the same 200 out-of-distribution samples to establish a baseline. Perhaps unsurprisingly, none of the methods are able to consistently outperform the expert policy in most tasks. We notice that KODex is able to outperform the baselines in Tool Use and Door Opening tasks, while NGF performs better in Object Relocation and In-Hand Reorientation tasks.

D. Robustness to changes in physical properties

This experiment is motivated by the fact that sim-to-real transfer often involves changes in physical properties. Further consistent use of robotic hardware could result in changes to physical properties. We evaluate the robustness of the reference dynamics learned by each method to changes in hand mass or object mass for the Object Relocation task. Specifically, we consider three variations: i) *Heavy Object*: 0.18 (default) → 1.88 (new), ii) *Light Hand*: 4.0 (default) → 3.0 (new), and iii) *Heavy Hand*: 4.0 (default) → 5.0 (new). We are not including a variation involving a lighter object as we found that this variation did not impact the performance of the default controller.

TABLE II: Robustness to variations in the physical properties

Success Rate (%)	Variation	Heavy Object	Light Hand	Heavy Hand
Controller				
Expert agent	77.0	100.0	100.0	
Noisy expert agent	0.0	47.0	56.5	
KODex + Original controller	19.5	82.5	21.5	
KODex + Expert-tuned controller	34.0	85.0	89.0	
KODex + Noisy-expert-tuned controller	24.5	77.5	63.5	
NDP + Original controller	13.5(±5.0)	72.1(±9.6)	31.6(±10.0)	
NDP + Expert-tuned controller	19.9(±5.8)	63.2(±15.0)	92.4(±1.2)	
NDP + Noisy-expert-tuned controller	23.6(±8.1)	66.8(±8.1)	42.5(±18.0)	
NGF + Original controller	25.8(±4.9)	96.6(±0.97)	19.3(±3.8)	
NGF + Expert-tuned controller	52.6(±3.9)	95.6(±2.2)	94.5(±0.9)	
NGF + Noisy-expert-tuned controller	32.8(±5.5)	82.4(±2.0)	57.3(±12.2)	

It is important to note we held the reference dynamics learned by each method constant for this experiment, irrespective of the changes to the hand or the object. Instead, we relearned two tracking controllers, each using 200 rollouts from either the expert agent or a noisy expert agent, following the procedure detailed in Section. IV-C.

In Table. II, we report the task success rate of KODex, NDP, and NGF policies (all trained on 200 demonstrations) before and after relearning the controller. We also report the task success rate of both noiseless and noisy expert agents to establish baselines. It is no surprise that all methods suffer a drop in performance when using the original controller. For the Light Hand variation, the original controller already shows good performance, so the relearned controllers have little to offer in terms of task success rate. In contrast, all methods clearly benefit from relearning the controller in the Heavy Object and Heavy Hand variations, evidenced by the increased task success rate. We also see that all methods struggle to regain the similar task success rate in the Heavy Object variation compared to Heavy Hand variation, perhaps due to the complexity of learning to grasp a considerably heavier object. Though these methods with the controllers tuned by the noisy expert perform worse than the ones trained by the expert, they are still able to outperform the noisy expert itself.

These results demonstrate that changes to the robot/system dynamics (e.g., due to the sim-to-real gap) can be handled

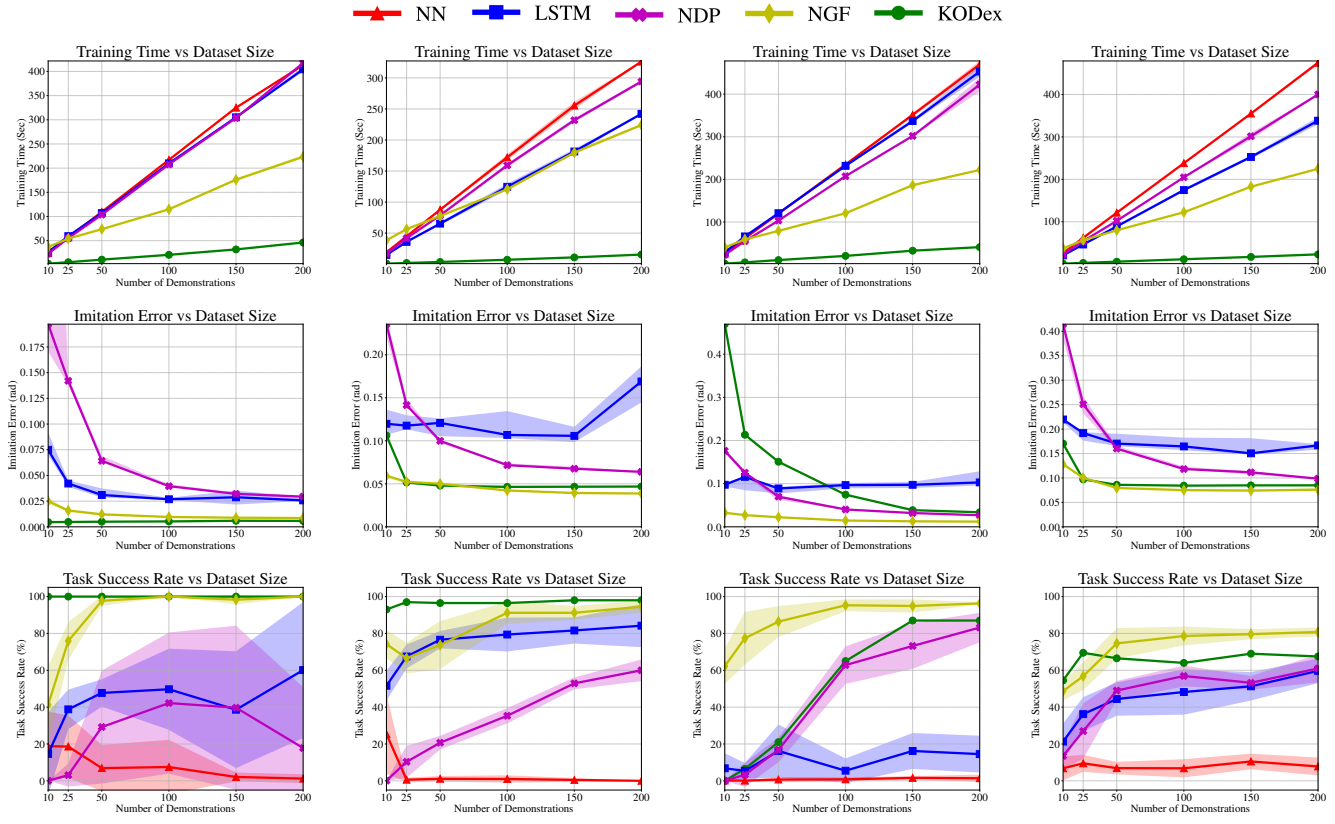


Fig. 4: The effects of the number of demonstrations on training time (the top row), the imitation error (the middle row), and the task success rate (the bottom row). Solid lines are the mean values and the shaded areas show mean \pm standard deviation, over five random seeds for each demonstration size. Note that we did not plot NN's imitation errors as they were out of scale.

in a task-agnostic way by fine tuning the tracking controller, without the need for relearning the reference dynamics. Further, once again, we observe that KODex is able to perform comparably to SOTA approaches despite its simplicity.

VII. CONCLUSIONS AND LIMITATIONS

In this work, we investigate the utility of Koopman operator theory in learning dexterous manipulation skills. To this end, we contribute a new imitation learning framework dubbed as KODex that can learn complex dexterous manipulation skills as linear dynamical systems in higher-dimensional spaces. Our experimental results conclusively demonstrate that Koopman operator theory offers a unique set of advantages over existing learning-based approaches. Specifically, we show that KODex can i) analytically learn dexterous manipulation skills, eliminating the sensitivity to parameter initialization and reducing the need for significant user expertise, ii) match or outperform SOTA imitation learning approaches on various dexterous manipulation tasks, while being an order of magnitude more computationally efficient.

While our work offers considerable promise for the utility of Koopman-operator theory in dexterous manipulation, it reveals numerous avenues for improvement and future research. First, KODex has limited capacity for out-of-distribution generaliza-

tion in its current form. This necessitates the need for additional training data collected offline or online using approaches like DAGGER [33]. Future work can also investigate if out-of-distribution generalization can be improved by swapping the polynomial lifting functions with learned lifting functions [34–36], allowing for end-to-end policy learning. Second, we did not deploy KODex on physical hardware. Although our results on robustness to changes in physical properties show promise, we plan to deploy KODex on different physical platforms to evaluate if it can learn to control physical robots. Third, Koopman operators can be used to learn system dynamics via self play to enable model-based reinforcement learning. Fourth, policies learned using KODex can be subject to rigorous theoretical analysis, thanks to its linear dynamical system. For instance, a recently-discovered connection between contraction analysis and Koopman operator theory [37] can help derive convergence and stability guarantees on learned policies.

REFERENCES

- Allison M Okamura, Niels Smaby, and Mark R Cutkosky. An overview of dexterous manipulation. In *Proceedings 2000 ICRA. Millennium Conference. IEEE International Conference on Robotics and Automation. Symposia Pro-*

ceedings (Cat. No. 00CH37065), volume 1, pages 255–262, 2000.

[2] OpenAI, Marcin Andrychowicz, Bowen Baker, Maciek Chociej, Rafal Jozefowicz, Bob McGrew, Jakub Pachocki, Arthur Petron, Matthias Plappert, Glenn Powell, Alex Ray, Jonas Schneider, Szymon Sidor, Josh Tobin, Peter Welinder, Lilian Weng, and Wojciech Zaremba. Learning Dexterous In-Hand Manipulation. arXiv, 2018. doi: 10.48550/ARXIV.1808.00177.

[3] Anusha Nagabandi, Kurt Konolige, Sergey Levine, and Vikash Kumar. Deep dynamics models for learning dexterous manipulation. In *Conference on Robot Learning*, pages 1101–1112. PMLR, 2020.

[4] Mandy Xie, Ankur Handa, Stephen Tyree, Dieter Fox, Harish Ravichandar, Nathan D Ratliff, and Karl Van Wyk. Neural geometric fabrics: Efficiently learning high-dimensional policies from demonstration. In *6th Annual Conference on Robot Learning*.

[5] B. O. Koopman. Hamiltonian Systems and Transformation in Hilbert Space. *Proceedings of the National Academy of Sciences*, 17(5):315–318, 1931. doi: 10.1073/pnas.17.5.315. URL <https://www.pnas.org/doi/abs/10.1073/pnas.17.5.315>.

[6] Aravind Rajeswaran, Vikash Kumar, Abhishek Gupta, Giulia Vezzani, John Schulman, Emanuel Todorov, and Sergey Levine. Learning Complex Dexterous Manipulation with Deep Reinforcement Learning and Demonstrations. In *Proceedings of Robotics: Science and Systems (RSS)*, 2018.

[7] Harish Ravichandar, Athanasios S. Polydoros, Sonia Chernova, and Aude Billard. Recent advances in robot learning from demonstration. *Annual Review of Control, Robotics, and Autonomous Systems*, 3(1):297–330, 2020.

[8] Auke Jan Ijspeert, Jun Nakanishi, Heiko Hoffmann, Peter Pastor, and Stefan Schaal. Dynamical movement primitives: learning attractor models for motor behaviors. *Neural computation*, 25(2):328–373, 2013.

[9] S Mohammad Khansari-Zadeh and Aude Billard. Learning stable nonlinear dynamical systems with gaussian mixture models. *IEEE Transactions on Robotics*, 27(5):943–957, 2011.

[10] Klaus Neumann and Jochen J Steil. Learning robot motions with stable dynamical systems under diffeomorphic transformations. *Robotics and Autonomous Systems*, 70:1–15, 2015.

[11] Harish Ravichandar, Iman Salehi, and Ashwin Dani. Learning Partially Contracting Dynamical Systems from Demonstrations. In *Proceedings of the 1st Annual Conference on Robot Learning*, volume 78, pages 369–378, 13–15 Nov 2017.

[12] M Asif Rana, Anqi Li, Harish Ravichandar, Mustafa Mukadam, Sonia Chernova, Dieter Fox, Byron Boots, and Nathan Ratliff. Learning reactive motion policies in multiple task spaces from human demonstrations. In *Conference on Robot Learning*, pages 1457–1468. PMLR, 2020.

[13] Muhammad Asif Rana, Anqi Li, Dieter Fox, Byron Boots, Fabio Ramos, and Nathan Ratliff. Euclideanizing flows: Diffeomorphic reduction for learning stable dynamical systems. In *Learning for Dynamics and Control*, pages 630–639. PMLR, 2020.

[14] Nadia Figueroa and Aude Billard. Locally active globally stable dynamical systems: Theory, learning, and experiments. *The International Journal of Robotics Research*, 41(3):312–347, 2022.

[15] Shikhar Bahl, Mustafa Mukadam, Abhinav Gupta, and Deepak Pathak. Neural dynamic policies for end-to-end sensorimotor learning. In *NeurIPS*, 2020.

[16] Tao Chen, Jie Xu, and Pulkit Agrawal. A System for General In-Hand Object Re-Orientation. In *5th Annual Conference on Robot Learning*, 2021.

[17] Haozhi Qi, Ashish Kumar, Roberto Calandra, Yi Ma, and Jitendra Malik. In-hand object rotation via rapid motor adaptation. *arXiv preprint arXiv:2210.04887*, 2022.

[18] Henry Zhu, Abhishek Gupta, Aravind Rajeswaran, Sergey Levine, and Vikash Kumar. Dexterous manipulation with deep reinforcement learning: Efficient, general, and low-cost. In *2019 International Conference on Robotics and Automation (ICRA)*, pages 3651–3657. IEEE, 2019.

[19] Takayuki Osa, Joni Pajarinen, Gerhard Neumann, J Andrew Bagnell, Pieter Abbeel, Jan Peters, et al. An algorithmic perspective on imitation learning. *Foundations and Trends® in Robotics*, 7(1-2):1–179, 2018.

[20] Sridhar Pandian Arunachalam, Irmak Güzey, Soumith Chintala, and Lerrel Pinto. Holo-dex: Teaching dexterity with immersive mixed reality. *arXiv preprint arXiv:2210.06463*, 2022.

[21] Vikash Kumar, Abhishek Gupta, Emanuel Todorov, and Sergey Levine. Learning dexterous manipulation policies from experience and imitation. *arXiv preprint arXiv:1611.05095*, 2016.

[22] Peter Henderson, Riashat Islam, Philip Bachman, Joelle Pineau, Doina Precup, and David Meger. Deep reinforcement learning that matters. In *Proceedings of the AAAI conference on artificial intelligence*, volume 32, 2018.

[23] Ian Abraham, Gerardo De La Torre, and Todd D Murphrey. Model-based control using Koopman operators. *arXiv preprint arXiv:1709.01568*, 2017.

[24] Ian Abraham and Todd D. Murphrey. Active Learning of Dynamics for Data-Driven Control Using Koopman Operators. *IEEE Transactions on Robotics*, 35(5):1071–1083, 2019. doi: 10.1109/TRO.2019.2923880.

[25] Daniel Bruder, Brent Gillespie, C David Remy, and Ram Vasudevan. Modeling and control of soft robots using the koopman operator and model predictive control. *arXiv preprint arXiv:1902.02827*, 2019.

[26] Daniel Bruder, Xun Fu, R. Brent Gillespie, C. David Remy, and Ram Vasudevan. Koopman-Based Control of a Soft Continuum Manipulator Under Variable Loading Conditions. *IEEE Robotics and Automation Letters*, 6(4):6852–6859, 2021. doi: 10.1109/LRA.2021.3095268.

[27] Matthew O Williams, Ioannis G Kevrekidis, and Clarence W Rowley. A data–driven approximation of the koopman operator: Extending dynamic mode decomposition. *Journal of Nonlinear Science*, 25(6):1307–1346, 2015.

[28] Josiah P Hanna and Peter Stone. Grounded action transformation for robot learning in simulation. In *Thirty-first AAAI conference on artificial intelligence*, 2017.

[29] Xue Bin Peng, Erwin Coumans, Tingnan Zhang, Tsang-Wei Lee, Jie Tan, and Sergey Levine. Learning agile robotic locomotion skills by imitating animals. *arXiv preprint arXiv:2004.00784*, 2020.

[30] Faraz Torabi, Garrett Warnell, and Peter Stone. Recent advances in imitation learning from observation. *arXiv preprint arXiv:1905.13566*, 2019.

[31] Todorov, Emanuel and Erez, Tom and Tassa, Yuval. Mujoco: A physics engine for model-based control. In *2012 IEEE/RSJ International Conference on Intelligent Robots and Systems*, pages 5026–5033, 2012.

[32] Ajay Mandlekar, Danfei Xu, Josiah Wong, Soroush Nasiriany, Chen Wang, Rohun Kulkarni, Li Fei-Fei, Silvio Savarese, Yuke Zhu, and Roberto Martín-Martín. What matters in learning from offline human demonstrations for robot manipulation. *arXiv preprint arXiv:2108.03298*, 2021.

[33] Stéphane Ross, Geoffrey Gordon, and Drew Bagnell. A reduction of imitation learning and structured prediction to no-regret online learning. In *Proceedings of the fourteenth international conference on artificial intelligence and statistics*, pages 627–635. JMLR Workshop and Conference Proceedings, 2011.

[34] Matthias Weissenbacher, Samarth Sinha, Animesh Garg, and Kawahara Yoshinobu. Koopman q-learning: Offline reinforcement learning via symmetries of dynamics. In *International Conference on Machine Learning*, pages 23645–23667. PMLR, 2022.

[35] Bethany Lusch, J Nathan Kutz, and Steven L Brunton. Deep learning for universal linear embeddings of nonlinear dynamics. *Nature communications*, 9(1):1–10, 2018.

[36] Yunzhu Li, Hao He, Jiajun Wu, Dina Katabi, and Antonio Torralba. Learning compositional koopman operators for model-based control. In *International Conference on Learning Representations*, 2020. URL <https://openreview.net/forum?id=H1ldzA4tPr>.

[37] Bowen Yi and Ian R. Manchester. On the Equivalence of Contraction and Koopman Approaches for Nonlinear Stability and Control. In *2021 60th IEEE Conference on Decision and Control (CDC)*, pages 4609–4614, 2021. doi: 10.1109/CDC45484.2021.9683450.

[38] Klaus Greff, Rupesh K Srivastava, Jan Koutník, Bas R Steunebrink, and Jürgen Schmidhuber. Lstm: A search space odyssey. *IEEE transactions on neural networks and learning systems*, 28(10):2222–2232, 2016.

[39] Karl Van Wyk, Man Xie, Anqi Li, Muhammad Asif Rana, Buck Babich, Bryan Peele, Qian Wan, Iretiayo Akinola, Balakumar Sundaralingam, Dieter Fox, et al. Geometric fabrics: Generalizing classical mechanics to capture the physics of behavior. *IEEE Robotics and Automation Letters*, 2022.

[40] Ching-An Cheng, Mustafa Mukadam, Jan Issac, Stan Birchfield, Dieter Fox, Byron Boots, and Nathan Ratliff. RMPflow: A geometric framework for generation of multi-task motion policies, 2020.

APPENDICES

A. State Design

In this section, we show the state design for each task in detail. It should be noted that the motion capability of the hand for each task were suggested from the work [6] that originally introduced these tasks. For a decent implementation, we employed the same setting.

Tool use For this task, the floating wrist base can only rotate along the x and y axis, so we have $\mathbf{x}_r(t) \in \mathcal{X}_r \subset \mathbb{R}^{26}$. Regarding the object states, unlike the other tasks, where the objects of interest are directly manipulated by the hand, this task requires to modify the environment itself. As a result, except for the hammer positions, orientations and their corresponding velocities $\mathbf{p}_t^{\text{tool}}, \mathbf{o}_t^{\text{tool}}, \dot{\mathbf{p}}_t^{\text{tool}}, \dot{\mathbf{o}}_t^{\text{tool}}$ (\mathbb{R}^3), we also define the nail goal position \mathbf{p}^{nail} (\mathbb{R}^3). Finally, we have $\mathbf{x}_o(t) = [\mathbf{p}_t^{\text{tool}}, \mathbf{o}_t^{\text{tool}}, \dot{\mathbf{p}}_t^{\text{tool}}, \dot{\mathbf{o}}_t^{\text{tool}}, \mathbf{p}^{\text{nail}}] \in \mathcal{X}_o \subset \mathbb{R}^{15}$. As a result, $\mathbf{x}(t)$ includes 41 states in total and we use $T = 100$.

Door opening For this task, the floating wrist base can only move along the direction that is perpendicular to the door plane but rotate freely, so we have $\mathbf{x}_r(t) \in \mathcal{X}_r \subset \mathbb{R}^{28}$. Regarding the object states, we define the fixed door position \mathbf{p}^{door} , which can provide with case-specific information (similar to \mathbf{p}^{nail} in Tool Use), and the handle positions $\mathbf{p}_t^{\text{handle}}$ (both \mathbb{R}^3). In order to take into consideration the status of door being opened, we include the angular velocity of the opening angle $v_t(\mathbb{R}^1)$. Finally, we have $\mathbf{x}_o(t) = [\mathbf{p}_t^{\text{handle}}, v_t, \mathbf{p}^{\text{door}}] \in \mathcal{X}_o \subset \mathbb{R}^7$. As a result, $\mathbf{x}(t)$ includes 35 states in total and we use $T = 70$.

Object relocation For this task, the ADROIT hand is fully actuated, so we have $\mathbf{x}_r(t) \in \mathcal{X}_r \subset \mathbb{R}^{30}$ (24-DoF hand + 6-DoF floating wrist base). Regarding the object states, we define $\mathbf{p}^{\text{target}}$ and $\mathbf{p}_t^{\text{ball}}$ as the target and current positions. Then, we compute $\bar{\mathbf{p}}_t^{\text{ball}} = \mathbf{p}_t^{\text{ball}} - \mathbf{p}^{\text{target}}$, which is the component of $\mathbf{p}_t^{\text{ball}}$ in a new coordinate frame that is constructed by $\mathbf{p}^{\text{target}}$ being the origin. We additional include the ball orientation $\mathbf{o}_t^{\text{ball}}$ and their corresponding velocities $\dot{\mathbf{p}}_t^{\text{ball}}, \dot{\mathbf{o}}_t^{\text{ball}}$ (all \mathbb{R}^3). Finally, we have $\mathbf{x}_o(t) = [\bar{\mathbf{p}}_t^{\text{ball}}, \mathbf{o}_t^{\text{ball}}, \dot{\mathbf{p}}_t^{\text{ball}}, \dot{\mathbf{o}}_t^{\text{ball}}] \in \mathcal{X}_o \subset \mathbb{R}^{12}$. As a result, $\mathbf{x}(t)$ includes 42 states in total and we use $T = 100$.

In-hand reorientation For this task, the floating wrist base is fixed, so we only consider the 24-DoF hand joints. Therefore, we have $\mathbf{x}_r(t) \in \mathcal{X}_r \subset \mathbb{R}^{24}$. Regarding the object states, we define \mathbf{o}^{goal} and $\mathbf{o}_t^{\text{pen}}$ as the goal and current pen orientations, which are both unit direction vectors. Then, we transform $\mathbf{o}_t^{\text{pen}}$ to a new rotated coordinate frame that is constructed by \mathbf{o}^{goal} being x axis ([1,0,0]). Note that the vector $\bar{\mathbf{o}}_t^{\text{pen}}$ after transformation is also a unit vector and it converges to x axis if the pen is perfectly manipulated to goal orientation \mathbf{o}^{goal} . In addition, we also include the center of mass position $\mathbf{p}_t^{\text{pen}}$ and their corresponding velocities $\dot{\mathbf{p}}_t^{\text{pen}}, \dot{\mathbf{o}}_t^{\text{pen}}$ (all \mathbb{R}^3). Finally, we have $\mathbf{x}_o(t) = [\mathbf{p}_t^{\text{pen}}, \bar{\mathbf{o}}_t^{\text{pen}}, \dot{\mathbf{p}}_t^{\text{pen}}, \dot{\mathbf{o}}_t^{\text{pen}}] \in \mathcal{X}_o \subset \mathbb{R}^{12}$. As a result, $\mathbf{x}(t)$ includes 36 states in total and we use $T = 100$.

In this work, we only included the joint positions as the robot states (with the only exception of NGF's second-order policy) for the following reasons: 1) Given that these tasks are not repetitive, we found that joint position information was sufficient to disambiguate the robot's next action, 2) even

when ambiguity arises for a given joint position, object state information can help with disambiguation. Further, the impressive performance achieved by KODex in our experiments support this design choice. Indeed, KODex is agnostic to this specific state design. One can incorporate velocity information into the robot state space without the need of any changes to the training procedure.

B. Task Success Criteria

The quantitative criteria of task successes are listed below. We used the same settings as in the paper [6].

Tool Use: The task is considered successful if at last time step T , the Euclidean distance between the final nail position and the goal nail position is smaller than 0.01.

Door Opening: The task is considered successful if at last time step T , the door opening angle is larger than 1.35 rad.

Object Relocation: At each time step t , if $\sqrt{|\mathbf{p}^{\text{target}} - \mathbf{p}_t^{\text{ball}}|^2} < 0.10$, then we have $\rho(t) = 1$. The task is considered successful if $\sum_{t=1}^T \rho(t) > 10$.

In-hand Reorientation: At each time step t , if $\mathbf{o}^{\text{goal}} \cdot \mathbf{o}_t^{\text{pen}} > 0.90$ ($\mathbf{o}^{\text{goal}} \cdot \mathbf{o}_t^{\text{pen}}$ measures orientation similarity), then we have $\rho(t) = 1$. The task is considered successful if $\sum_{t=1}^T \rho(t) > 10$.

C. Sampling Procedure

We describe the sampling procedure in this section. The sample distributions used for RL training and demo collection were identical, which was also suggested in [6]. For out-of-distribution data, we generated them to evaluate the generalizability of each policy.

Tool Use: We randomly sampled the nail heights (h) from a uniform distributions. Within distribution: we used $h \in \mathcal{H} \sim \mathcal{U}(0.1, 0.25)$; Out of distribution: we used $h \in \mathcal{H} \sim \mathcal{U}(0.05, 0.1) \cup \mathcal{U}(0.25, 0.3)$.

Door Opening: We randomly sampled the door positions (xyz) from uniform distributions. Within distribution: we used $x \in \mathcal{X} \sim \mathcal{U}(-0.3, 0)$, $y \in \mathcal{Y} \sim \mathcal{U}(0.2, 0.35)$, and $z \in \mathcal{Z} \sim \mathcal{U}(0.252, 0.402)$; Out of distribution: we used $y \in \mathcal{Y} \sim \mathcal{U}(0.1, 0.2)$ (x, z remained unchanged).

Object Relocation: We randomly sampled the target positions (xyz) from uniform distributions. Within distribution: we used $x \in \mathcal{X} \sim \mathcal{U}(-0.25, 0.25)$, $y \in \mathcal{Y} \sim \mathcal{U}(-0.25, 0.25)$, and $z \in \mathcal{Z} \sim \mathcal{U}(0.15, 0.35)$; Out of distribution: we used $z \in \mathcal{Z} \sim \mathcal{U}(0.35, 0.40)$ (x, y remained unchanged).

In-hand Reorientation: We randomly sampled the pitch (α) and yaw (β) angles of the goal orientation from uniform distributions. Within distribution: we used $\alpha \in \mathcal{A} \sim \mathcal{U}(-1, 1)$ and $\beta \in \mathcal{B} \sim \mathcal{U}(-1, 1)$; Out of distribution: we used $\alpha \in \mathcal{A} \sim \mathcal{U}(-1.2, -1) \cup \mathcal{U}(1, 1.2)$ and $\beta \in \mathcal{B} \sim \mathcal{U}(-1.2, -1) \cup \mathcal{U}(1, 1.2)$.

D. Policy Design

We show the detailed policy design in this section. All the baseline policies were trained to minimize the trajectory reproduction error.

KODex: The representation of the system is given as: $\mathbf{x}_r = [x_r^1, x_r^2, \dots, x_r^n]$ and $\mathbf{x}_o = [x_o^1, x_o^2, \dots, x_o^m]$ and superscript

is used to index states. The details of the state design for each task is provided in Appendix. VII-A. In experiments, the vector-valued lifting functions ψ_r and ψ_o in (10) were polynomial basis function defined as

$$\begin{aligned}\psi_r &= \{x_r^i x_r^j\} \cup \{(x_r^i)^3\} \text{ for } i, j = 1, \dots, n \\ \psi_o &= \{x_o^i x_o^j\} \cup \{(x_o^i)^2 (x_o^j)\} \text{ for } i, j = 1, \dots, m\end{aligned}\quad (13)$$

Note that $x_r^i x_r^j / x_r^j x_r^i$ only appears once in lifting functions (similar to $x_o^i x_o^j / x_o^j x_o^i$), and we ignore t as the lifting functions are the same across the time horizon.

The choice of lifting functions can be viewed as the hyper-parameter of KODex. We make this choice as inspired from [23] and experimental results also indicate its effectiveness. Through all the experiments, we stucked with the same set of lifting functions, which helped to relieve us from extensive efforts of tuning the hyper-parameters, e.g. network layer size, that were necessary for baseline policies as shown in Appendix. VII-E.

Full-connected Neural Network (NN): The first baseline is a feedforward network that ingests the states $x(1)$ and iteratively produces the predictions $x(t)$, $t = 2, \dots, T$ via the rollout of a Multilayer Perceptron (MLP). The reference joint trajectories ($x_r(t)$) are then used to execute the robot with the learned controller C . The significance of this baseline is to evaluate a policy that produces a high-dimensional motion without any additional structure.

Long Short-Term Memory (LSTM): We create an LSTM-based policy under the same input-output flow as the NN policy. We also apply two fully-connected layers between the task input/output and the input/hidden state of the LSTM network. Similarly, the same controller C is deployed to track the reference joint trajectory. LSTM networks are known to be beneficial to imitation learning [32] and suitable for sequential processing [38], e.g. motion generation. Therefore, we expect to evaluate the performance of the recurrent structures in these tasks.

Neural Dynamic Policy (NDP): The Neural Dynamic Policy [15] embeds desired dynamical structure as a layer in neural networks. Specifically, the parameters of the second order Dynamics Motion Primitives (DMP) are predicted as outputs of the preceding layers (MLP in [15]). As a result, it allows the overall policy easily reason in the space of trajectories and can be utilized for learning from demonstration. We train an NDP policy following the imitation learning pipeline described in [15]. For each task, given $x(1)$, the neural network components in NDP generate the parameters of DMPs (radial basis functions (RBFs) in [15]), which are forward integrated to produce the reference joint trajectories for tracking.

Neural Geometric Fabrics policy (NGF): The Neural Geometric Fabrics [4], a structured policy class, that enables efficient skill learning for dexterous manipulation from demonstrations by leveraging structures induced by Geometric Fabrics [39]. Geometric Fabrics is a stable class of the Riemannian Motion Policy (RMP) [40]. It has been demonstrated that NGF outperforms RMP in policy learning for dexterous manipulation task in [4]. The NGF policy is defined in the configuration

space of the robot, which is composed of a geometric policy, a potential policy and a damping term. More specifically, the NGF policy is constructed as follows: (1) define a geometric policy pair $[\mathbf{M}, \pi]$ and a potential policy pair $[\mathbf{M}_f, \pi_f]$ in the configuration space \mathbf{q} , (2) energize the geometric policy (project orthogonal to the direction of motion with \mathbf{p}_e) to create a collection of energy-preserving paths (the Geometric Fabric), and (3) force the Geometric Fabric with a potential defined by $[\mathbf{M}_f, \pi_f]$ and damp via b applied along $\dot{\mathbf{q}}$, which ensures convergence to the potential's minima. The potential policy π_f is the gradient of a function of position only. Note that we parameterize the geometric policy pair $[\mathbf{M}, \pi]$, the potential policy pair $[\mathbf{M}_f, \pi_f]$, and the damping scalar b with MLP networks and learn them from demonstration data.

E. Optimizing baseline model size

As described in Appendix. VII-D, we stucked with the same set of lifting functions for KODex and report the task success rate when we trained KODex on training set and tested it on validation set in Table. III. However, for baselines, the hyper-parameters were selected through a set of ablation experiments for each task using the training set over three choices of model size, including small size, median size and large size. We generated five random seeds for parameter initialization per model size, per baseline, and per task, as all learning based baseline models are sensitive to parameter initialization [22]. For each baseline policy, we report the mean and standard deviation of the task success rate on the validation set over five random seeds in Table. IV V VI VII.

Based on these results, we selectd the model size that offers the best performance in terms of task success rate. In addition, these results indicate that, unlike KODex, extensive hyper-parameter tuning and various trials on parameter initialization for baseline models are necessary. Note that we use l to denote $\dim(x(t))$.

TABLE III: Task success rate on validation set (KODex)

Tool	Door	Relocation	Reorientation
100.0%	96.0%	88.0%	62.0%

TABLE IV: Hyper-parameters on NN Network Sizes

Success Rate (%)	Task	Tool	Door	Relocation	Reorientation
Model Size					
MLP: (32, 64, 32)	0.4(±0.8)	0.0(±0.0)	0.4(±0.8)	6.8(±3.9)	
MLP: (64, 128, 64)	0.0(±0.0)	0.4(±0.8)	1.2(±2.4)	10.4(±6.6)	
MLP: (128, 256, 128)	0.0(±0.0)	0.0(±0.0)	0.8(±1.6)	6.0(±1.5)	

TABLE V: Hyper-parameters on LSTM Network Sizes

Success Rate (%)	Task	Tool	Door	Relocation	Reorientation
Model Size					
LSTM: 200 fc: (l , 100), (200, l)	28.8(±25.0)	87.6(±10.3)	7.6(±5.9)	56.4(±7.4)	
LSTM: 250 fc: (l , 175), (250, l)	60.8(±36.6)	80.8(±24.5)	7.6(±7.5)	48.0(±17.0)	
LSTM: 300 fc: (l , 250), (300, l)	44.8(±31.8)	82.0(±13.9)	16.4(±14.5)	54.0(±11.0)	

TABLE VI: Hyper-parameters on NDP Network Sizes

Success Rate (%)	Task	Tool	Door	Relocation	Reorientation
Model Size					
MLP: (32, 64, 32) 10 RBFs		0.0(± 0.0)	8.0(± 2.5)	30.0(± 9.3)	57.2(± 8.6)
MLP: (64, 128, 64) 20 RBFs		16.8(± 29.8)	40.8(± 8.1)	74.0(± 4.9)	59.2(± 6.5)
MLP: (128, 256, 128) 30 RBFs		18.4(± 31.9)	66.0(± 5.2)	79.2(± 7.7)	62.4(± 7.8)

TABLE VII: Hyper-parameters on NGF Network Sizes

Success Rate (%)	Task	Tool	Door	Relocation	Reorientation
Model Size					
MLP: (64, 32)		99.2(± 1.6)	87.2(± 12.0)	87.6(± 8.5)	77.6(± 2.3)
MLP: (128, 64)		100.0(± 0.0)	90.0(± 5.9)	94.4(± 3.2)	72.4(± 4.5)
MLP: (256, 128)		83.6(± 20.1)	90.8(± 4.3)	95.2(± 1.6)	78.4(± 3.4)

F. Hyper-parameters for controller learning

The hyper-parameters we used to learn the inverse dynamics controller C for each task were the same as listed in Table. VIII. Note that we use l_r to denote $\dim(\mathbf{x}_r(t))$.

TABLE VIII: Hyper-parameters on controller learning

Hidden Layer	Activation	Learning Rate	Iteration
$(4l_r, 4l_r, 2l_r)$	ReLU	0.0001	300